HHS Public Access

Author manuscript

Eur J Med Chem. Author manuscript; available in PMC 2020 February 01.

Published in final edited form as:

Eur J Med Chem. 2019 February 01; 163: 853–863. doi:10.1016/j.ejmech.2018.12.022.

Unprecedented inhibition of P-gp activity by a novel rutheniumcyclopentadienyl compound bearing a bipyridine-biotin ligand

Leonor Côrte-Real[a], **Brittany Karas**[b,c], **Patrícia Gírio**[a,d], **Alexis Moreno**[d], **Fernando Avecilla**[e], **Fernanda Marques**[f], **Brian T. Buckley**[b], **Keith R. Cooper**[c], **Cathleen Doherty**[b], **Pierre Falson**[d], **M. Helena Garcia**[a], and **Andreia Valente**[a]

[a]Centro de Química Estrutural, Faculdade de Ciências da Universidade de Lisboa, Campo Grande, 1749-016 Lisboa, Portugal.

[b]Environmental and Occupational Health Sciences Institute, Rutgers University, 170 Frelinghuysen Road, Piscataway NJ, 08854, U.S.A.

[c]Department of Biochemistry and Microbiology, Rutgers University, 76 Lipman Drive, New Brunswick NJ, 08854, U.S.A.

[d]Drug Resistance and Membrane Proteins Team, Molecular Biology and Structural Biochemistry Laboratory, UMR 5086 CNRS-UCBL1, IBCP 7 Passage du Vercors, 69 367 Lyon Cedex 07 France.

[e]Grupo Xenomar, Centro de Investigacións Científicas Avanzadas (CICA), Departamento de Química, Facultade de Ciencias, Universidade da Coruña, Campus de A Coruña, 15071 A Coruña, Spain.

[f]Centro de Ciências e Tecnologias Nucleares, Instituto Superior Técnico, Universidade de Lisboa, Estrada Nacional 10, km 139.7, 2695-066 Bobadela LRS, Portugal

Abstract

Two new ruthenium complexes, $[Ru(\eta^5\text{-}Cp)(PPh_3)(2,2'\text{-bipy-}4,4'\text{-}R)]^+$ with R = CH_2OH (**Ru1**) or dibiotin ester (**Ru2**) were synthesized and fully characterized. Both compounds were tested against two types of breast cancer cells (MCF7 and MDA-MB231), showing better cytotoxicity than cisplatin in the same experimental conditions. Since multidrug resistance (MDR) is one of the main problems in cancer chemotherapy, we have assessed the potential of these compounds to overcome resistance to treatments. **Ru2** showed exceptional selectivity as P-gp inhibitor, while **Ru1** is possibly a substrate. *In vivo* studies in zebrafish showed that **Ru2** is well tolerated up to 1.17 mg/L, presenting a LC_{50} of 5.73 mg/L at 5 days post fertilization.

Graphical Abstract

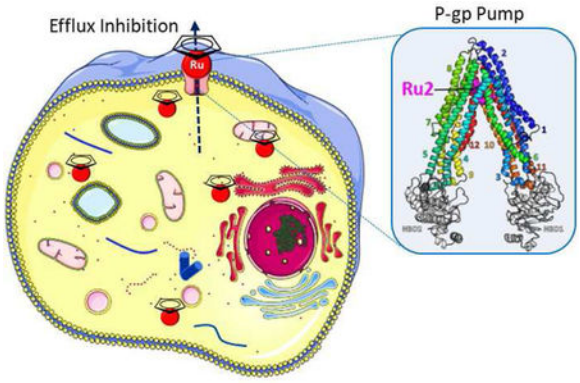

Keywords

Ruthenium organometallic compounds; anticancer agents; P-gp inhibitor; multidrug resistance

Introduction

A major concern regarding chemotherapy, the first line treatment for many cancers, is the development of drug resistant phenotypes that considerably limit the efficiency of the drugs. Drug resistance might be either inherent (*i.e.* at the first treatment) or acquired (*i.e.* after subsequent treatments). In fact, multidrug resistance (MDR) is one of the major clinical obstacles in cancer chemotherapy, being responsible for more than 90 % of treatment failures of metastatic cancer using adjuvant chemotherapy.[1] One of the most common MDR mechanisms is the overexpression of adenosine triphosphate (ATP)-binding cassette (ABC) superfamily transporters, which mediate the efflux of anticancer drugs thus lowering their intracellular concentrations under effective amounts. Among these ABC transporters the P-glycoprotein (P-gp, *ABCB1*), Breast Cancer Resistance Protein (BCRP, *ABCG2*), Multidrug Resistance Protein 1 (MRP1, *ABCC1*) and Multidrug Resistance Protein 2 (MRP1, *ABCC2*) have been reported to play important roles in inducing MDR in several cancers, such as lung, breast, colon, ovarian cancers and melanomas.

P-gp is one of the most studied pumps as a drug target for the treatment of multidrug resistant cancers. Some studies have shown that modifications on the structure of known anticancer compounds, such as anthracyclines and taxanes confer the ability to overcome P-gp transport.[2] Despite promising *in vitro* results claiming new strategies to overcome the MDR issue, clinical trials remain disappointing.[3,4] A recent approach is the development of anticancer agents that would also behave as MDR inhibitors. For example, a series of aminated thioxanthones were tested for *in vitro* activity as antitumor agents and P-gp inhibitors.[5] The overall results, highlighted two compounds (1-[2-(1H-benzimidazol-2-yl)ethanamine]-4-propoxy-9H-thioxanthen-9-one and 1-{[2(4-nitrophenyl)ethyl]amino}−4-propoxy-9H-thioxanthen-9-one) with a dual action as Pgp inhibitors and cytotoxic agents.[5]

During the last decade we have been developing new $[RuCpR(PPh_3)(bipyridine\text{-}R')]^+$ (CpR = η^5-C_5H_5 or η^5-$C_5H_4(CH_3)$, R' = -H, -CH_3, -CH_2OH, - OC_3H_6-C_8F_{17}) compounds as anticancer agents.[6–13] These compounds are highly cytotoxic against a wide panel of

cancer cell lines with different degrees of aggressiveness, stable under physiologic conditions and their cell uptake and cellular distribution is dependent on the substituents of the bipyridine ligand. Recently we tested some of those compounds bearing 2,2'bipyridine-4,4'-subtituints as MDR inhibitors.[7] The overall results showed that the compounds bearing the bipyridines with -H and -CH_2OH substituents were poor substrates to the main MDR human pumps, while the bipyridine with -CH_3 as substituent displayed inhibitory properties for MRP1 and MRP2 pumps. All compounds showed very good cytotoxicity for ovarian cancer cells (sensitive and resistant) with IC_{50} values surpassing up to 120 times those of cisplatin in the same experimental conditions.

In this paper, the effect of the addition of biotin, vitamin B7, to the $[Ru(\eta^5C_5H_5)(PPh_3)(bipyridine\text{-}R)]^+$ scaffold (R = -CH_2OH, **Ru1** or dibiotin ester, **Ru2**) is explored in terms of MDR potential. Indeed, several compounds with anticancer activity have been functionalized with biotin to improve their efficiency and efficacy.[14] The new biotinylated compound toxicity was also evaluated using a modified embryo larval zebra fish model (OECD. 2013).

Results and Discussion

Synthesis and characterization of Ruthenium compounds

Mononuclear cationic complexes of the general formula $[Ru(\eta^5\text{-}Cp)(PPh_3)(2,2'\text{-}bipy4,4'\text{-}R)]^+$ with R = -CH_2OH (**Ru1**) or dibiotin ester (**Ru2**),were prepared, as shown in Scheme 1.

Sigma coordination of bidentate *N,N* chelating 2,2'-bipy-4,4'-R ligand to ruthenium was achieved in good yields by halide abstraction from the starting material $[Ru(\eta^5Cp)(PPh_3)_2Cl]$ using silver triflate. Purification of the organometallic complexes was achieved by slow diffusion recrystallization from dichloromethane/*n*-hexane and THF/*n*-hexane. The formulation and purity of the new complexes and of the dibiotin ester are supported by FT-IR, UV-vis and ^1H, ^{13}C, and ^{31}P NMR spectroscopic data and elemental analyses.

The dibiotin ester was synthesized following a slightly modified literature protocol.[15] Instead of using the *N,N'*-dicyclohexylcarbodiimide (DCC) as a coupling agent for the esterification reaction, a different approach using *N*-(3-Dimethylaminopropyl)-*N*′ethylcarbodiimide hydrochloride (EDC) was tested. In fact, the main problem with DCC is the formation of a water insoluble urea byproduct very difficult to be eliminated. This alternative synthesis is done in a one-pot reaction, avoids the use of high temperatures and longtime reactions and allows a simpler purification of the final product.

The esterification reaction between 4,4′-dihydroxymethyl-2,2′-bipyridine and biotin was followed by ^1H-NMR spectroscopy. An evident deshielding of H_6 protons has occurred as expected due to the presence of oxygen atoms from the ester and the signal multiplicity also changed from duplet to singlet. Both signals from the -OH of the alcohol and carboxylic acid of the biotin have disappeared, confirming the successful esterification.

The FT-IR spectra of the dibiotin ester also confirms a successful esterification by the typical stretching frequency for the υ (C=O) of the ester at 1732 cm^{-1}.

The analysis of the solid-state FT-IR spectra of the organometallic rutheniumcyclopentadienyl derivatives **Ru1** and **Ru2** shows the presence of the typical bands expected for υ_{CH} stretching of the bipyridine, phosphane and cyclopentadienyl ligands in the range 3080–3060 cm^{-1} as well as the bands for $\upsilon_{C=C}$ at 1600–1400 cm^{-1}. The presence of the triflate counterion was revealed in the typical range for this group (~1240 cm^{-1}), which agrees with the cationic character of the compounds. The hydroxyl groups of the bpy(CH_2OH) were also found at 3410 cm^{-1} for **Ru1**.

Analysis of the overall ^1H NMR spectra shows a general deshielding of the η^5-C_5H_5 protons upon coordination of the bipyridine-based ligands, as expected for a cationic species. The bipyridine protons show a deshielding on the *ortho* protons (~0.6 ppm) and a shielding on the *meta* protons (−0.5 ppm and −0.3 ppm, for **Ru1** and **Ru2**, respectively), giving evidence of successful coordination of the bipyridyl derivative to the metal center. The results are in accordance with the previous discussed effects in the ^1H NMR analysis. All the detailed spectroscopic data concerning the ^{13}C NMR experiments are in the experimental section. The ^{31}P NMR spectra showed a single sharp singlet resonance corresponding to the coordinated phosphane co-ligand (~51 ppm). A deshielding behavior upon coordination was expected as it is in accordance with its **σ** donor character.

The electronic spectra of both complexes and the bipyridine ligands were recorded in 10^{-5}-10^{-3} M dichloromethane solutions. Figure 1 presents the electronic spectra of both compounds. In addition to the strong absorption bands, characteristic of each bipyridyl derivative and the {[Ru(Cp)(PPh_3)]$^+$} organometallic fragment (appearing below 300 nm), the electronic spectra of these compounds were characterized essentially by one broad, medium-strength, absorption band with a shoulder in the visible region (400 – 600 nm) with $\varepsilon_{max} \sim 4 \times 10^3$ M^{-1} cm^{-1} that can be related to metal-to-ligand charge transfer bands (MLCT), from Ru 4d to **π*** N-heteroaromatic rings and to phosphane, as previously reported for related compounds.[7]

[Ru(η^5-C_5H_5)(PPh_3)(4,4’-diyldimethanol-2,2’-bipyridine)][CF_3SO_3] **Ru1** crystallized from methanol/ether solution as orange prisms (crystal dimensions 0.37 × 0.25 × 0.10 mm). Figure 2A shows an ORTEP representation of [Ru(η^5-C_5H_5)(PPh_3)(4,4’diyldimethanol-2,2’-bipyridine)]$^+$ of **Ru1**. In **Ru1**, the asymmetric unit contains one cationic ruthenium complex and one $CF_3SO_3^-$ anion. In the molecular structure, the ruthenium center adopts a “piano stool” distribution formed by the ruthenium-Cp unit bound to phosphane and to nitrogen atoms of the 4,4’-diyldimethanol-2,2’-bipyridine ligand. One phosphane group occupies the other coordination position. The distance for Ru-P bond is Ru(1)-P(1) = 2.3098(8) Å. The distances for Ru-N bonds are Ru(1)-N(1) 2.087(3) Å and Ru(1)-N(2) 2.080(3) Å. The distance between Ru and the centroid of the **π**-bonded cyclopentadienyl moiety is 1.8301(1) Å to Ru center (ring slippage 0.033 Å). The mean value of the Ru-C bond distance is 2.1906(30) Å. Table 1 contains selected bond lengths and angles for **Ru1**. **π**-**π** stacking interactions are present in the structure. Comparing it with the already published [RuCp(2,2’-bipyridine)PPh_3]$^+$ cation,[10] the distance between the bipyridine ligand ring N(1)-C(6)-C(7)-C(8)-C(9)-C(10) and the phosphane phenyl ring C(30)-C(31)-C(32)-C(33)-C(34)-C(35) are similar (3.695(3) Å for **Ru1**, see Figure 2B, and 3.744(2) Å for [RuCp(2,2’-bipyridine)PPh_3]$^+$).

X-ray structure analysis of **Ru1** shows two enantiomers of cation complex [Ru($\eta^5C_5H_5$)(PPh_3)(4,4'-diyldimethanol-2,2'-bipyridine)]$^+$ of **Ru1** in the racemic crystal (space group P 1), the chirality being due to a twist of the PPh_3 and Cp units. The cation complex [Ru(η^5-C_5H_5)(PPh_3)(4,4'-diyldimethanol-2,2'-bipyridine)]$^+$ of **Ru1** presents a mirror plane which contain P, Ru and the centroid of Cp ring (see Figure S1).[11,16] Hydrogen bonds between hydroxy groups and $CF_3SO_3^-$ anions are present in the crystal packing (see Table 2).

Stability studies in aqueous media

Stability is a key issue when assessing the biological activity of any metallodrug. Thus, the stability of the compounds was evaluated as the absorbance variation percentage in the cell culture medium DMEM (Dulbecco's Modified Eagle Medium) containing up to 5% DMSO to allow for the solubilization of the compounds in an adequate concentration for optical electronic spectra. Both compounds are stable under these conditions allowing for their further study in human cancer cells (Figure S2).

Biological Evaluation of the compounds

Cytotoxicity in breast cancer cell lines—The cytotoxicity of the ruthenium complexes **Ru1** and **Ru2** was studied on two human cancer cell lines with different degrees of aggressiveness (breast MCF7 and MDA-MB-231) using the colorimetric MTT assay. Cells were incubated with each compound, in a concentration range of 1 μM to 100 μM, for a period of 24 hours. Table 3 summarizes the IC_{50} values obtained.

Both compounds are cytotoxic against the two cell lines tested and 2–13 times more cytotoxic than cisplatin under the same experimental conditions. **Ru1** is more cytotoxic than **Ru2** by ~7-fold for the MCF7 cancer cell line. Both compounds are equally cytotoxic for the MDA-MB-231 cancer cell line.

Effect of Ruthenium compounds on cells overexpressing ABC transporters—One major limitation in chemotherapy is the acquired resistance that cancer cells might develop. Thus, within this work our goals were to examine if ABC pumps are able to pump the compounds out of cells leading to their inefficacy or if **Ru1** and **Ru2** can act as ABC transporters inhibitors. These proteins are overexpressed in cancer cell lines and allow the efflux of the drug out from the cell. To avoid this efflux, the identification of selective inhibitors that block the drugs efflux is being explored. Table 4 presents the cytotoxic activity of the ruthenium complexes **Ru1** and **Ru2** for the noncancerous (or "normal") cell lines. The HEK293 cells were either wild-type (WT, transformed with an empty vector) or transfected with a plasmid containing a gene coding for the transporter proteins: BCRP, MRP1, MRP2. NIH3T3 cells were used in the same way to express the P-gp.

Ru1 differentially inhibited the growth of control cells, with IG_{50} below 7 μM for HEK293 cells and of 28 μM for NIH3T3 cells. The expression of MRP1 or BCRP in HEK293 cells increased the IG_{50} of **Ru1** to 10 and 19 μM, respectively; it also increased to about 70 μM for NIH3T3 cells expressing P-gp, which represents concentrations 2, 2.8 and 2.4 times higher than for the respective non-transfected cells. These results suggest that **Ru1** is transported by these pumps, leading to higher resistance profiles. As cancer cells are

susceptible to overexpress these ABC transporters, **Ru1** may not be considered as a good potential chemotherapeutic agent.

Ru2 showed IG_{50} between 1 and 6 μM for HEK293 cells without significant differences when MRP1, MRP2 or BCRP are expressed. **Ru2** is also much more efficient than **Ru1** on NIH3T3 cells with an IG_{50} of 7 μM, again without any difference when P-gp is expressed. These results make **Ru2** a potential chemotherapeutic agent as none of these transporters confers resistance against its cytotoxic action.

Another aim of this study was to determine if **Ru1** and **Ru2** inhibit the MDR pumps, thus improving their chemotherapy efficiency. We measured by flow cytometry the intracellular accumulation of fluorescent substrates co-incubated with **Ru1** or **Ru2**, in P-gp-, MRP1-, MRP2- or BCRP-transfected cells. Results are displayed in Figure 3. As shown and as expected, **Ru1** did not display any inhibition property of the MDR pumps. On the contrary, **Ru2** efficiently blocked the efflux of rhodamine 123 mediated by P-gp. This was specific of P-gp as the efflux of other substrates mediated by BCRP, MRP1 or MRP2 were not modified by **Ru2**.

Molecular Docking—While **Ru1** was found to be a substrate of P-gp, interestingly **Ru2** was found to be an inhibitor of the same transporter despite similar structure. To better characterize this behavior at the molecular level, we performed flexible molecular docking for both compounds on a human P-gp 3D model generated by us. Fifty-five residues, which form the drug-binding pocket, were made flexible and 10 poses per molecule were generated. Both **Ru1** and **Ru2** best pose (Figure 4A) dock at the same upper part of the drugbinding pocket. Although it is also true for all other poses (Figure 4B), **Ru2** seems much more stabilized as the structures colored in magenta and orange almost share the same position between them, while it is not the case for the common structure in **Ru1**. The R-group of **Ru2** can, however, adopt many positions. As **Ru1** has been shown to be a substrate and **Ru2** an inhibitor, we hypothesized that **Ru1** structure binds into the pocket, induces a conformational change and is transported by P-gp. The addition of long biotin-group allows **Ru2** to interact with more residues and prevents any further conformational change of P-gp. This finding is supported by a gain of affinity of −3.5 $kcal.mol^{-1}$ for **Ru2** best pose compared to **Ru1**, leading to a significantly high theoretical affinity of −18.1 $kcal.mol^{-1}$ with P-gp (Figure 4C).

In vivo toxicity assessment using zebrafish embryos—The zebrafish has been used as an experimental model to study chemical toxicity since the 1950s. Additionally, this model allows for examining adverse outcome pathways from biochemical to whole organism endpoints, unlike cell culture and more expensive rodent models.

The zebrafish has proven to be a valuable vertebrate model for assessing chemical toxicity and studying chemical mechanisms of toxicity. The zebrafish embryo larval assay (ELA) offers certain advantages over traditional vertebrate models, including rapid generation time, high fecundity, external embryonic development, capacity for high stocking density in relatively small areas, and lower maintenance costs.[18,19] A modified OECD.2013 protocol was used as previously described.[20] The ELA allows establishment of testable

hypotheses for evaluating adverse outcome pathways from the subcellular to the organ system level. This makes the zebrafish model ideal for anticancer drug research where one of the objectives is to identify adverse effects of chemical exposure.

Zebrafish embryos were used as a model for the *in vivo* toxicity evaluation of the most promising compound, **Ru2**. At 3 hours post fertilization (hpf) eggs were exposed to increasing concentrations of **Ru2**. The concentrations collected and analytically evaluated at the end of the experiment were determined to be 0.00, 0.15, 0.47, 1.17, 2.18, 3.48, 4.24, 5.12 and 6.57 mg/L. Daily observations of the embryos were recorded and included lethality/survival as well as lesions (such as pericardial sac edema, yolk sac edema, and malformations) were evaluated. The fertilization rate was >80 % and the control survival rate was consistently >90 %.

Four acute toxicity endpoints were obtained from the dose response curves: lethality for 50 % of the embryos or larvae - LC_{50}, NOEC – no observed effect concentration, LOEC – lowest observed effect concentration and NOAEL – No observed adverse effect level. (Table 5). It should be noted that the NOAEL is based on the dose of the compound found within the whole tissue of the zebrafish, while the other values were determined from the exposure medium. Graphical representations of the lethality-response curve and the evolution of lethality through time can be seen in Figure 5 and Figure S3, respectively. The lethality-response curve distribution for **Ru2** compound (Figure 5) allowed the accurate estimation of the LC_{50} value. At the end of the 120 hpf experiment, the living larvae were sacrificed, digested with a mixture of nitric acid and hydrogen peroxide and then analyzed by ICP-MS to quantify the ruthenium in ng per larvae, as shown in Table 5 and Figure 6.

For the last three doses administered (3.48, 4.24, 5.12 mg/L) the Ru mass per larvae was approximately the same, ~3.7 ng indicating a threshold tolerance for **Ru2**. The exact delivered doses of **Ru2** to the larvae for each concentration are shown in Figure S4. During the 5-day experiment, morphological lesions involving multiple tissues and organ systems were observed following **Ru2** exposure. The morphological lesions included curved spine/tail malformation, yolk sac and pericardial sac edema, cranial malformation and underdeveloped eyes. These lesions were observed in zebrafish exposed to **Ru2** starting from 2.18 to 5.12 mg/L. The most frequently observed grossly visible effects are summarized in Figure 7 and Table S2.

To better characterize adverse morphometric effects, endpoints such as intraocular distance, total body length, pericardial sac and yolk sac area were assessed. Intraocular distance was used to indicate changes in cranio-facial development following embryonic **Ru2** exposure. The three highest concentrations of the compound tested (3.48, 4.24 and 5.12 mg/L) resulted in a significant decrease of intraocular distance which agrees with the underdeveloped eye and altered cranium structure.

The total body length measurement was used to determine if exposure to **Ru2** during the embryonic life stages influenced larval growth. This compound caused significantly reduced body length following exposure to ≥ 1.17 mg/L with no significant differences observed at the first two lower doses (0.15 and 0.47 mg/L, respectively); an indication that this

compound inhibits the overall growth of the organism. The observed curved tail and cranial abnormalities further support a skeletal impact. In higher vertebrates this might manifest itself in improper bone formation and skeletal abnormalities especially in utero and early juvenile development.

The pericardium is anterior to the yolk sac. The pericardial membrane surrounds the atrium and ventricle of the heart muscle and when fluid accumulates in this area, pericardial sac edema is observed (Figure 7A). Measuring the pericardial sac size is a common biomarker for a compromised cardiovascular system. The **Ru2** compound caused a significantly increased pericardial sac size at both 2.18 mg/L and 5.12 (highest concentration), whereas no significant differences were observed for the lower concentrations.

The yolk sac is comprised of vitellogenin derived yolk-proteins, maternally supplied by the oocyte to fully support nutritional needs of the embryo/larvae prior to beginning feeding after 120 hpf. Measuring the yolk sac size is an important endpoint in determining whether the compound affected the volume of the available nutrients and their utilization in embryonic zebrafish. It was observed that the yolk sac size increased with increasing concentration of **Ru2**, which may indicate that the nutrients are not being taken up by the larvae. This data agrees with the yolk sac edema lesion observed for the highest concentration (Figure 7B). Yolk sac edema is not synonymous with yolk sac megaly. The edema is due to fluid accumulating outside the vasculature and the increased size is more indicative of an uptake of lipoproteins from the yolk sac.

Conclusions

Two structurally related compounds $[Ru(\eta^5\text{-}Cp)(PPh_3)(2,2'\text{-bipy-}4,4'\text{-}R)]^+$ (with R = CH_2OH, **Ru1** or dibiotin ester, **Ru2**) were successfully synthesized. **Ru1** crystallizes in a centrosymmetric triclinic $P\bar{1}$ space group as enantiomer. Both compounds are cytotoxic against two different breast cancer cell lines, with IC_{50} better than cisplatin, and are among the best Ru organometallic compounds tested under the same experimental conditions[21–27]. While **Ru1** was found to be a substrate for ABC transporters, **Ru2** showed a remarkable selective inhibition for P-gp, showing promising results as a cytotoxic agent since none of the tested transporters confers resistance against its cytotoxic action. This is the first ruthenium organometallic compound showing P-gp inhibition, as far as we are aware, from the few results reported in the literature.[28,29] **Ru2** is well tolerated in zebrafish up to 1.17 mg/L. The LC_{50} was found to be 5.73 mg/L at 5 days post fertilization.

Overall, comparing the structures of **Ru1** and **Ru2**, it seems that the addition of a long leg-like chemical group to a substrate might be a powerful tool to create new inhibitors of ABC transporters. The potential of **Ru2** as metallodrug will be further explored in order to unveil its mechanisms of action.

Experimental section

General procedures

All reactions and manipulations were performed under nitrogen atmosphere using *Schlenk* techniques. All solvents used were dried and freshly distilled under nitrogen prior to use,

using standard methods. ^{1}H, ^{13}C, and ^{31}P NMR spectra were recorded on a Bruker Avance 400 spectrometer at probe temperature using commercially available deuterated solvents. ^{1}H and ^{13}C chemical shifts (s = singlet; d = duplet; t = triplet; m = multiplet) are reported in parts per million (ppm) downfield from internal standard Me_4Si and the ^{31}P NMR spectra are reported in ppm downfield from external standard, 85% H_3PO_4. Coupling constants are reported in Hz. All assignments were attributed using COSY, HMBC and HMQC NMR techniques. Infrared spectra were recorded on KBr pellets using a Mattson Satellite FT-IR spectrophotometer and only relevant bands were cited in the text. Electronic spectra were obtained at room temperature on a Jasco V-560 spectrometer from solutions of 10^{-3}-10^{-5} M in quartz cuvettes (1 cm optical path). Elemental analyses were performed at *Laboratório de Análises, at Instituto Superior Técnico*, using a Fisons Instruments EA1 108 system. Data acquisition, integration and handling were performed using a PC with the software package EAGER-200 (Carlo Erba Instruments).

Synthesis

2,2'-bipyridine-4,4'-dibiotin ester (bipy-biotin)—The synthesis of the ligand bipy-biotin was done following a modified literature procedure.[15]

The synthesis was performed by addition of 4,4´-dihydroxymethyl-2,2´-bipyridine (0.150 g, 0.69 mmol), 5-[(3aS,4S,6aR)-2-oxohexahydro-1H-thieno[3,4-d] imidazol-4yl]pentanoic acid (biotin) (0.424 g, 1.74 mmol) and 4-dimethylaminopyridine (DMAP; 0.085 g; 0.69 mmol) in dimethylformamide (DMF; 10 mL) to a stirred solution and with ice/water bath (0 °C). Then *N*-(3-Dimethylaminopropyl)-*N*′-ethylcarbodiimide hydrochloride (EDC) was added (0.333 g; 1.735 mmol), to the colorless solution obtained and continue to stir for 30 minutes with the ice/water bath. After the 30 minutes, the bath was removed, and the solutions remained stirring all night at room temperature. On the next day the solvent was removed under vacuum and washed twice with water and diethyl ether and dried overnight.

Yield: 60 %; white powder. ^{1}H NMR - [DMSO-d^6, Me_4Si, δ/ppm]: 8.68 [d, 2, $^{3}J_{HH}$ = 4.8, H_1], 8.37 [s, 2, H_4], 7.43 [d, 2, $^{3}J_{HH}$ = 4.8, H_2], 6.45 [s, 2, NH], 6.37 [s, 2, NH], 5.25 [s, 4, H_6], 4.28 [t, 4, $^{3}J_{HH}$ = 6,8, H_{15}], 4.11 [t, 4, $^{3}J_{HH}$ = 4, H_{13}), 3.08 (m, 2, H_{12}), 2.80 (dd, 2, $^{3}J_{HH}$ = 4.0, $^{3}J_{HH}$ = 4.0, H_{16}), 2.57 [d, 2, $^{3}J_{HH}$ = 12.4, H_{16}], 2.44 [t, 4, $^{3}J_{HH}$ = 7.2, H_8], 1.61 [m, 4, H_9], 1.48 [m, 4, H_{11}], 1.36 [m, 4, H_{10}]. UV-Vis- [DMSO, λ_{max}/nm (ε/$M^{1}cm^{-1}$)]: 286 (9495). FTIR [KBr, cm^{-1}]: 3385, 3238 ($_{N-H}$ amine), 3082 (υ_{C-H} aromatic), 2935, 2862 ($_{C-H}$ alkanes), 1732 ($_{C=O}$ ester), 1705 ($\upsilon_{C=O}$ ketone). Elemental analysis calc. for $C_{32}H_{40}N_6O_6S_2$ (668.83 g/mol): C: 57.47, H: 6.03, N: 12.57, S: 9.59. Found: C: 57.01, H: 6.19, N: 12.47, S: 9.34.

[Ru(η^5-Cp)(PPh_3)(2,2'-bipyridine-4,4'-dimethanol)][CF_3SO_3] (Ru1)—To a stirred suspension of 0.36 g (0.5 mmol) of [Ru(η^5-Cp)(PPh_3)$_2$Cl] in dichloromethane (30 mL), 0.13 (0.6 mmol) of 2,2'-bipyridine-4,4'-dimethanol were added followed by addition of 0.153 g (0.6 mmol) of $AgCF_3SO_3$. After refluxing for a period of 4 h the color changed slightly from orange to a darker orange. The reaction mixture was cooled down to room temperature and the solution was filtered to eliminate the AgCl and PPh_3 precipitates. The solvent was then

removed under vacuum. **Ru1** was recrystallized once from dichloromethane/*n*-hexane and a second time from methanol/diethyl ether solution originating orange crystals.

Yield = 50 %. ^{1}H NMR - [MeOD, Me_4Si, δ/ppm]: 9.21 [d, 2, $^{3}J_{HH}$ = 4.0, H_1], 7.92 [s, 2, H_4], 7.36 [t, 3, $^{3}J_{HH}$ = 8.0, $H_{para}(PPh_3)$], 7.25 [m, 8, H_2+$H_{meta}(PPh_3)$], 7.01 [t, 6, $^{3}J_{HH}$ = 8.0, $H_{ortho}(PPh_3)$], 4.74 [s, 5, η^5-C_5H_5], 4.69 [s, 4, C_6]. ^{13}C NMR [MeOD, Me_4Si, δ/ppm]: 156.9, 156.8 (C_1+C_3), 153.5 (C_5); 134.1 ($^{2}J_{CP}$ = 11, C_{ortho}-PPh_3); 133.1, 132.7 (Cq, PPh_3); 131.2 ($^{4}J_{CP}$ = 2, C_{para}-PPh_3); 129.5 ($^{3}J_{CP}$ = 10, C_{meta}-PPh_3); 123.5 (C_2); 121.3 (C_4); 79.29 ($^{2}J_{CP}$ = 2, η^5-C_5H_5); 62.72 (C_6). ^{31}P NMR [MeOD, δ/ppm): 51.15 (s, PPh_3). UV-Vis in CH_2Cl_2, λ_{max}/nm (ε/$M^{-1}cm^{-1}$): 473 (*Sh*), 414 (4026), 352 (*Sh*), 292 (20719). FTIR [KBr, cm^{-1}]: 3410 (υ_{O-H}), 3078–3057 (υ_{C-H} Cp and aromatic rings), 2850 (υ_{C-H} alkanes), 1616 and 1479 ($\upsilon_{C=C}$), 1248 ($\upsilon(CF_3SO_3^-)$), 1223 (υ_{C-O}). Elemental analysis (%) Found: C, 53.7; H, 4.1; N, 3.4; S, 4.0. Calc. for $C_{36}H_{32}N_2PF_3O_5SRu$: C, 54.5; H, 4.1; N, 3.5; S, 4.0. ESI-MS (+): calc. for [**Ru1**]$^{+}$ m/z: 645.12, found m/z: 644.91.

[Ru(η^5-Cp)(PPh_3)(bipy-biotin)][CF_3SO_3] (Ru2)—To a stirred and degassed solution of [Ru(η^5-Cp)(PPh_3)$_2$Cl] (0.353 g, 0.49 mmoles) in methanol (40 mL) was added $AgCF_3SO_3$ (0.125 g, 0.49 mmoles). The resulting mixture was stirred for 1 h at room temperature followed by the addition of bipy-biotin (0.250 g, 0.37 mmoles). After an 6 h reflux the reaction mixture was cooled to room temperature, filtered and the solvent was removed under vacuum. Orange crystalline powder was obtained after recrystallization from dichloromethane/*n*-hexane and THF/*n*-hexane.

Yield: 86 %. ^{1}H NMR - [$(CD_3)_2CO$, Me_4Si, δ/ppm]: 9.50 [d, 2, $^{3}J_{HH}$ = 4.0, H_1], 8.11 [s, 2, H_4], 7.43 [m, 4, $H_{para}(PPh_3)$], 7.33 [m, 9, $H_{meta}(PPh_3)$ + H_2], 7.12 [t, 6, $^{3}J_{HH}$ = 8.0, $H_{ortho}(PPh_3)$], 6.20 [d, 2, *J* = 16.0, NH], 6.16 [s, 2, NH], 5.25 [d, 4, $^{2}J_{HH}$ = 4.0, H_6], 4.93 [s, 5, η^5-C_5H_5], 4.50 [m, 2, H_{15}], 4.33 [m, 2, H_{13}], 3.22 [m, 2, H_{12}], 2.94 [m, 2, H_{16}], 2.69 [t, 2, $^{3}J_{HH}$ = 12, H_{16}], 2.51 [m, 4, H_8], 1.74 [m, 4, H_9], 1.64 [m, 4, H_{11}], 1.49 [m, 4, H_{10}]. ^{13}C NMR [$(CD_3)_2CO$, δ/ppm]: 173.6 (C_7), 164.1 (C_{14}), 157.1 (C_1), 156.5 (C_5), 147.6 (C_3), 134.0 ($^{2}J_{CP}$ = 11, C_{ortho}-PPh_3), 132.4 ($^{1}J_{CP}$ = 41, C*q*, PPh_3), 131.2 ($^{4}J_{CP}$ = 1, C_{para}-PPh_3), 129.5 ($^{3}J_{CP}$ = 9, C_{meta}-PPh_3), 124.6 ($^{4}J_{CP}$ = 8, C_2), 122.6 ($^{4}J_{CP}$ = 11, C_4), 79.54 ($^{2}J_{CP}$ = 2, η^5-C_5H_5), 64.2 (C_6), 62.6 (C_{13}), 60.9 (C_{15}), 56.7 (C_{12}), 41.1 (C_{16}), 34.3 (C_8), 29.97 (under the signal of the solvent, C_{10}, C_{11}), 25.8 (C_9). ^{31}P NMR [$(CD_3)_2CO$, δ/ppm]: 51.2 (s, PPh_3). UV-vis [DMSO, λ_{max}/nm (ε x 10^3 / $M^{-1}cm^{-1}$)]: 296 (23.5), 353 (Sh), 430 (4.0), 486 (Sh). UV-vis [CH_2Cl_2, λ_{max}/nm (ε x 10^3/ $M^{-1}cm^{-1}$)]: 249 (Sh), 293 (21.7), 347 (Sh), 428 (4.2), 488 (Sh). FTIR [KBr, cm^{-1}]: 3074 (υ_{C-H} Cp and aromatic rings), 2929, 2860 (υ_{C-H} alkanes), 1736 ($\upsilon_{C=O}$ ester), 1701 ($\upsilon_{C=O}$ ketone), 1435 ($\upsilon_{C=C}$ Cp and aromatic rings), 1261 ($\upsilon(CF_3SO_3^-)$). Elemental analyses calc. for $C_{56}H_{60}F_3N_6O_9PRuS_3$ (1246.35 g/mol): C, 54.0; H, 4.9; N, 6.7; S, 7.7. Found: C, 53.9; H, 4.9; N, 6.2; S, 7.5. ESI-MS (+): calc. for [**Ru2**]$^{+}$ m/z: 1096.95, found m/z: 1097.28.

X-ray crystal structure determination—Three-dimensional X-ray data for [Ru(η^5-C_5H_5)(PPh_3)(4,4'-diyldimethanol-2,2'bipyridine)][CF_3SO_3] **Ru1** were collected on a Bruker SMART Apex CCD diffractometer at 100(2) K, using a graphite monochromator and Mo-K_α radiation (λ = 0.71073 Å) by the ϕ-ω scan method. Reflections were measured from a hemisphere of data collected of frames each covering 0.5 degrees in ω. Of the 265907

reflections measured in **Ru1**, all of which were corrected for Lorentz and polarization effects, and for absorption by semi-empirical methods based on symmetry-equivalent and repeated reflections, 8335 independent reflections exceeded the significance level $|F|/\sigma(|F|) > 4.0$, respectively. Complex scattering factors were taken from the program package SHELXTL.[30] The structure was solved by direct methods and refined by full-matrix least-squares methods on F^2. The non-hydrogen atoms were refined with anisotropic thermal parameters in all cases. Hydrogen atoms were located in difference Fourier map and left to refine freely, except for C(2S), C(3SA), C(3SB), C(3) and C(4), which were included in calculation positions and refined in the riding mode. A final difference Fourier map showed no residual density outside: 0.986 and −0.783 e.Å^{-3}. A weighting scheme $w = 1/[\sigma^2(F_o^2) + (0.049500\ P)^2 + 7.468500\ P]$ for **Ru1**, where $P = (|F_o|^2 + 2|F_c|^2)/3$, were used in the latter stages of refinement. The site occupancy factor was 0.45910 for C(3SA) and O(1SA). CCDC No. 1869965 contain the supplementary crystallographic data for **Ru1**. These data can be obtained free of charge via http://www.ccdc.cam.ac.uk/conts/retrieving.html, or from the Cambridge Crystallographic Data Centre, 12 Union Road, Cambridge CB2 1EZ, UK; fax: (+44) 1223–336-033; or e-mail: deposit@ccdc.cam.ac.uk. Crystal data and details of the data collection and refinement for the new compounds are collected in Table 6.

Stability studies in DMSO and DMSO/DMEM—For the stability studies, all complexes were dissolved in DMSO or 5% DMSO/95% DMEM at *ca.*1×10^{-4} M and their electronic spectra were recorded in the range allowed by the solvents at set time intervals.

Biological Evaluation

Cell lines and culture conditions—To evaluate the selectivity of the compounds on other ABC transporters, NIH3T3 parental cell line and NIH3T3/*ABCB1* drug resistant cell line transfected with human MDR1/A-G185, purchased from American Type Culture Collection (Manassas, VA) were used, as previously described.[31] HEK293 (Human embryonic kidney cell) were used to express the pcDNA3.1-h*ABCG2* plasmid[32] and Flp-In™−293 cells to express *ABCC1* and *ABCC2* genes transfected by electroporation using Neon® Transfection System (ThermoFisher scientific) with pcDNA5-FRT-*ABCC1* or pcDNA5-FRT-*ABCC2* respectively as previously described[33]. MCF7 and MDA-MB-231 breast cancer human tumor cell lines were obtained from ATCC.

Cells were grown at 37 ºC in 5% CO_2 in Dulbecco's modified Eagles's medium (DMEM high glucose) (PAA, GE Healthcare Life Sciences, Velizy-Villacoublay, France) supplemented with 10 % fetal bovine serum (FBS, PAA, GE Healthcare Life sciences, Velizy-Villacoublay, France), 1% penicillin / streptomycin (PAA, GE Healthcare Life sciences, Velizy-Villacoublay, France), with selection agent for the MRP1, MRP2, BCRP P-gp-transfected cell lines. The MCF7 and MDA-MB-231 cells were cultured in DMEM medium with 10% FBS and 1% penicillin/streptomycin.

All cells were adherent in monolayers and, upon confluence, were washed with phosphate buffer saline (PBS) 1x and harvested by digestion with trypsin 0.05% (v/v). Trypsin was inactivated by adding fresh complete culture media to the culture flask. Cells were then

suspended and transferred into new, sterile, culture flasks, or seeded in sterile test plates for the different assays.

All cells were manipulated under aseptic conditions in a flow chamber.

Compounds dilution and storage—All compounds were dissolved in DMSO and divided in aliquots of 10 μL each. After, they were store at −20 ºC until use.

Compound cytotoxicity evaluated by MTT assay—The cells were adherent in monolayers and, upon confluency, were harvested by digestion with trypsin-EDTA. The cytotoxicity of the complexes against the tumor cells was assessed using the colorimetric assay MTT (3-(4,5–2-yl)-2,5-ditetrazolium bromide), which measures conversion of the yellow tetrazolium into purple formazan by mitochondrial redox activity in living cells. For this purpose, cells (10–20 × 10^3 in 200 μL of medium) were seeded into 96-well plates and incubated in a 5% CO_2 incubator at 37 ºC. Cells were allowed to settle for 24 h followed by the addition of a dilution series of the complexes in medium (200 μL). The complexes (**Ru1** and **Ru2**) were first solubilized in DMSO, then in medium within the concentration range 0.1–100 μM. Cisplatin (the reference compound), was first solubilized in H_2O and then added at the same concentrations used for the ruthenium complexes. DMSO did not exceed 1% even for the higher concentration used and was without cytotoxic effect. After 24 h incubation (MDA-MB-231 and MCF7) or 48 h incubation (NIH3T3 and HEK293), the treatment solutions were removed by aspiration and MTT solution (200 μL, 0.5 mg/mL in PBS) was added to each well. After 3–4 h at 37 ºC/ 5% CO_2, the solution was removed, and the purple formazan crystals formed inside the cells were dissolved in DMSO (200 μL) by thorough shaking. The cellular viability was evaluated by measuring the absorbance at 570 nm by using a plate spectrophotometer.

Flow Cytometry—Cells were seeded at a density of 10^5 cells/well into 24-well culture plates. After a 24-hour incubation period, they were exposed to different concentrations of compounds and substrates for 30 minutes at 37 °C, 5% CO_2. After treatment, cells were washed with phosphate buffer saline (PBS) and detached from the plates with trypsin. Trypsin was neutralized with PBS-BSA 2% (Bovine Serum Albumin). Cells were then resuspended and transferred to cytometer tubes. The samples were kept on ice until analysis with a FACSCalibur cytometer (BD Biosciences, San Jose, CA, USA) or BD LSR-II system.

3D Modeling and docking studies—The human P-gp 3D model was based on the mouse P-gp structure (PDB 4q9h)[34] which shares 87% of sequence identity. Sequence alignment of the mouse P-gp (UniProtKB P21447) and human P-gp (UniProtKB P08183) was performed with the AlignMe server.[35] One model was chosen and refined between twenty generated with Modeller 9.19.[36] For docking experiment, the protein, flexible residues within the drug-binding pocket and ligands were prepared with AutoDockTools 4.[37,38] Computations were performed by Autodock Vina 1.1.2[39] to generate 10 poses per molecule with an exhaustiveness parameter of 32. As Autodock Vina does not support Ru atom (Rii = 2.96 Å, epsii = 0.056 kcal.mol^{-1}, vol =12.000 Å^3), it was replaced with F (Rii = 3.09 Å, epsii = 0.080 kcal.mol^{-1}, vol = 15.448 Å^3) which has the closest energy parameters

between all supported atoms, and then replaced back to Ru in resulting poses for visualization purpose.

In vivo toxicity assessment using zebrafish embryos.—The AB strain zebrafish (Zebrafish International Resource Center, Eugene, OR) was used for all experiments. Breeding stocks were bred and housed in Aquatic Habitats (Apopka, FL) recirculating systems under a 14/10 h light/dark cycle. System water was obtained by carbon/sand filtration of municipal tap water and water quality was maintained at <0.05 ppm nitrite, <0.2 ppm ammonia, pH between 7.2 and 7.7, and water temperature between 26 and 28 ºC. All experiments were conducted in accordance with the zebrafish husbandry protocol and embryonic exposure protocol (#08–025) approved by the Rutgers University Animal Care and Facilities Committee.

Males and females were maintained separately and co-mingled the night before to allow spawning the next morning. Spawning substrates were placed into the fish tanks on the day prior to spawning. In case eggs were obtained from more than one set of breeders all eggs that were fertilized and progressing normally through development were mixed. Zebrafish embryos were exposed to different concentrations of **Ru2** solutions (0.15, 0.47, 1.17, 2.18, 3.48, 4.24, 5.12, 6.57 mg/L) at 0.05 % of DMSO in individual glass vials through a waterborne exposure from 3 h postfertilization (hpf) until 120 hpf (5 days) in a static non-renewal protocol. The solutions were prepared from a Ru2 stock solution of 12.33 mg/L.

The exposure followed a modified OECD 236 protocol (OECD. 2013), where the endpoints of lesion presence, length and mortality were recorded, during the major stages of organ development and the toxicological estimates (LC_{50}, NOEC, LOEC and NOAEL) were determined. Those embryos surviving at the end of the toxicological experiment (120 hpf) were used for both morphological data and ICP-MS Ru quantification analysis.

For morphological data, approximately 12 individual larvae from each **Ru2** concentration and control group were fixed in formalin and then stained for bone and cartilage following a two-color acid free Alcian Blue/Alizarin red stain.[40] Photographs were taken using a Scion digital camera model CFW-1310C mounted on an Olympus SZ-PT dissecting microscope and cartilage/bone were measured using Adobe Photoshop. Endpoints examined included total body length, intraocular distance, and yolk sac size to assess larval growth, cranial facial development, and nutrient storage and usage, respectively (Supp.Inf. – Fig.S5).

For the analytical data, the solutions in each vial were collected for ICP-MS analysis and the larvae were euthanized and fixed with 10 % buffered formalin phosphate.[41]

Three replicates containing larvae from each concentration were also collected for ICPMS analysis (see below).

Each concentration of **Ru2** compound and corresponding control group was set up as individual experiments, and the sample size was between 30–40 embryos, and repeated two times. The controls had >90 % survival rate.

Quantification of ruthenium by Inductively coupled plasma mass spectrometry (ICP-MS)—Samples were quantified via high resolution ICP-MS (Nu Instruments Attom®, UK) at Rutgers EOHSI Analytical Facility. The instrument settings for the ICP-MS are provided in Table 7. Larval samples were microwave digested using a MARS X microwave digester (CEM Matthews NC) in OmniTrace® Nitric acid and diluted to 3.5% acid with 30 % hydrogen peroxide solution (Sigma-Aldrich). **Ru2** spiked egg water treatments were acidified to 3.5%. The samples were introduced through a ASX-500 Model 510 Auto Sampler (Cetac®) and into a Gass Expansion Conikal Nebulizer within the Peltier cooling system. Data was sent into the Attom software (Attolab v.1) and analyzed with NuQuant by using a seven-point calibration curve. The limit of quantification for these samples was 0.005 ppb and ruthenium isotopes 99, 100, 101, and 102 were quantified. It is important to note that an oxide of strontium, an ingredient in salt water solutions, like egg water, has considerable isobaric interference for ruthenium 100. No isobaric interferences were noted for larval samples. The ruthenium concentrations given by ICP-MS in μg/L (ppb) were converted to **Ru2** concentrations in mg/L.

Supplementary Material

Refer to Web version on PubMed Central for supplementary material.

Acknowledgements

This work was financed by the Portuguese Foundation for Science and Technology (Fundação para a Ciência e Tecnologia, FCT) within the scope of projects UID/QUI/00100/2013 and PTDC/QUI-QIN/28662/2017. Andreia Valente acknowledges the Investigator FCT2013 Initiative for the project IF/01302/2013 (acknowledging FCT, as well as POPH and FSE - European Social Fund). Leonor Côrte-Real thanks FCT for her Ph.D. Grant (SFRH/BD/100515/2014) and Fulbright Research Grant 2017/2018 with the support of FCT. Brittany Karas thanks NJAESRutgersNJ01201, NIEHS Training Grant T32-ES 007148 and Brian Buckley, Cathleen Doherty NIEHS P30 ES005022. Keith R. Cooper thanks NJAES Project 01202 (W2045), NIH ES005022. Patrícia Gírio was funded by the Erasmus + Program and a fellowship received from the French National Research Agency, ANR-13-BSV5–000101 (to Dr. Pierre Falson).

References

[1]. Pluchino KM, Hall MD, Goldsborough AS, Callaghan R, Gottesman MM, Collateral sensitivity as a strategy against cancer multidrug resistance, Drug Resist. Updat 15 (2012) 98–105. doi: 10.1016/j.drup.2012.03.002. [PubMed: 22483810]

[2]. Lehne G, P-glycoprotein as a Drug Target in the Treatment of Multidrug Resistant Cancer, Curr. Drug Targets 1 (2000) 85–99. doi:10.2174/1389450003349443. [PubMed: 11475537]

[3]. Takara K, Sakaeda T, Okumura K, An update on overcoming MDR1-mediated multidrug resistance in cancer chemotherapy., Curr. Pharm. Des 12 (2006) 273– 286. doi: 10.2174/138161206775201965. [PubMed: 16454744]

[4]. Wang J, Seebacher N, Shi H, Kan Q, Duan Z, Novel strategies to prevent the development of multidrug resistance (MDR) in cancer, Oncotarget 8 (2015) 84559–84571. doi:10.18632/oncotarget.19187.

[5]. Palmeira A, Vasconcelos MH, Paiva A, Fernandes MX, Pinto M, Sousa E, Dual inhibitors of P-glycoprotein and tumor cell growth: (Re)discovering thioxanthones, Biochem. Pharmacol 83 (2012) 57–68. doi:10.1016/j.bcp.2011.10.004. [PubMed: 22044878]

[6]. Matos A, Mendes F, Valente A, Morais T, Tomaz AI, Zinck P, Garcia MH, Bicho MB, Marques F, Ruthenium-Based Anticancer Compounds: Insights into Their Cellular Targeting and Mechanism of Action, in: and J.L.B.J. Holder Alvin A., Lilge Lothar, Browne Wesley R., Lawrence Mark

A.W.(Ed.), Ruthenium Complexes Photochem. Biomed. Appl, First Edit, 2018Wiley-VCH Verlag GmbH & Co. KGaA, 2018: pp. 201–219.

[7]. Côrte-Real L, Teixeira RG, Gírio P, Comsa E, Moreno A, Nasr R, Baubichon-Cortay H, Avecilla F, Marques F, Robalo MP, Mendes P, Ramalho JPP, Garcia MH, Falson P, Valente A, Methyl-cyclopentadienyl Ruthenium Compounds with 2,2′-Bipyridine Derivatives Display Strong Anticancer Activity and Multidrug Resistance Potential, Inorg. Chem 57 (2018). doi:10.1021/acs.inorgchem.8b00358.

[8]. Teixeira RG, Brás AR, Côrte-Real L, Tatikonda R, Sanches A, Robalo MP, Avecilla F, Moreira T, Garcia MH, Haukka M, Preto A, Valente A, Novel ruthenium methylcyclopentadienyl complex bearing a bipyridine perfluorinated ligand shows strong activity towards colorectal cancer cells, Eur. J. Med. Chem 143 (2018) 503–514. doi:10.1016/j.ejmech.2017.11.059. [PubMed: 29202411]

[9]. Côrte-Real L, Mendes F, Coimbra J, Morais TS, Tomaz AI, Valente A, Garcia MH, Santos I, Bicho M, Marques F, Anticancer activity of structurally related ruthenium(II) cyclopentadienyl complexes, J. Biol. Inorg. Chem 19 (2014) 853–867. doi:10.1007/s00775-014-1120-y. [PubMed: 24562604]

[10]. Moreno V, Font-Bardia M, Calvet T, Lorenzo J, Avilés FX, Garcia MH, Morais TS, Valente A, Robalo MP, DNA interaction and cytotoxicity studies of new ruthenium(II) cyclopentadienyl derivative complexes containing heteroaromatic ligands, J. Inorg. Biochem 105 (2011) 241–249. doi:10.1016/j.jinorgbio.2010.10.009. [PubMed: 21194624]

[11]. Côrte-Real L, Paula Robalo M, Marques F, Nogueira G, Avecilla F, Silva TJL, Santos FC, Isabel Tomaz A, Helena Garcia M, Valente A, The key role of coligands in novel ruthenium(II)-cyclopentadienyl bipyridine derivatives: Ranging from non-cytotoxic to highly cytotoxic compounds, J. Inorg. Biochem 150 (2015) 148–159. doi:10.1016/j.jinorgbio.2015.06.015. [PubMed: 26150132]

[12]. Valente A, Garcia MH, Marques F, Miao Y, Rousseau C, Zinck P, First polymer “ruthenium-cyclopentadienyl” complex as potential anticancer agent, J. Inorg. Biochem 127 (2013) 79–81. doi:10.1016/j.jinorgbio.2013.07.002. [PubMed: 23896008]

[13]. Morais TS, Valente A, Tomaz AI, Marques F, Garcia MH, Tracking antitumor metallodrugs: Promising agents with the Ru(II)- and Fe(II)cyclopentadienyl scaffolds, Future Med. Chem 8 (2016) 527–544. doi:10.4155/fmc.16.7. [PubMed: 27096164]

[14]. Mitra K, Shettar A, Kondaiah P, Chakravarty AR, Biotinylated Platinum(II) Ferrocenylterpyridine Complexes for Targeted Photoinduced Cytotoxicity, Inorg. Chem 55 (2016) 5612–5622. doi:10.1021/acs.inorgchem.6b00680. [PubMed: 27171926]

[15]. Haddour N, Gondran C, Cosnier S, A new biotinylated tris bipyridinyl iron (II) complex as redox biotin-bridge for the construction of supramolecular biosensing architectures, Time (2004) 324–325. doi:10.1039/b311566f.

[16]. Govindaswamy P, Linder D, Lacour J, Süss-Fink G, Therrien B, Chiral or not chiral? A case study of the hexanuclear metalloprisms [Cp(6)M(6)(micro(3)-tptkappaN)(2)(micro-C2O4-kappaO)(3)]6+ (M = Rh, Ir, tpt = 2,4,6-tri(pyridin-4yl)-1,3,5-triazine)., Dalton Trans 6 (2007) 4457–63. doi:10.1039/b709247d.

[17]. Côrte-Real L, Matos AP, Alho I, Morais TS, Tomaz AI, Garcia MH, Santos I, Bicho MP, Marques F, Cellular uptake mechanisms of an antitumor ruthenium compound: The endosomal/lysosomal system as a target for anticancer metal-based drugs, Microsc. Microanal 19 (2013) 1122–1130. doi:10.1017/S143192761300175X. [PubMed: 23790186]

[18]. Shive HR, Zebrafish Models for Human Cancer, Vet. Pathol 50 (2013) 468–482. doi:10.1177/0300985812467471. [PubMed: 23203679]

[19]. Sukardi H, Chng HT, Chan ECY, Gong Z, Lam SH, Zebrafish for drug toxicity screening: bridging the *in vitro* cell-based models and *in vivo* mammalian models, Expert Opin. Drug Metab. Toxicol 7 (2011) 579–589. doi:10.1517/17425255.2011.562197.

[20]. O. Guidelines, F.O.R. The, T. Of, Test No. 236: Fish Embryo Acute Toxicity (FET) Test, (2013) 1–22. doi:10.1787/9789264203709-en.

[21]. Morais TS, Santos FC, Jorge TF, Côrte-Real L, Madeira PJA, Marques F, Robalo MP, Matos A, Santos I, Garcia MH, New water-soluble ruthenium(II) cytotoxic complex: Biological activity

and cellular distribution, J. Inorg. Biochem 130 (2014) 1–14. doi:10.1016/j.jinorgbio.2013.09.013. [PubMed: 24145065]

[22]. Caruso F, Pettinari R, Rossi M, Monti E, Gariboldi MB, Marchetti F, Pettinari C, Caruso A, Ramani MV, Subbaraju GV, The in vitro antitumor activity of arene-ruthenium(II) curcuminoid complexes improves when decreasing curcumin polarity, J. Inorg. Biochem 162 (2016) 44–51. doi:10.1016/j.jinorgbio.2016.06.002. [PubMed: 27293144]

[23]. Ramadevi P, Singh R, Jana SS, Devkar R, Chakraborty D, Mixed ligand ruthenium arene complexes containing N-ferrocenyl amino acids: Biomolecular interactions and cytotoxicity against MCF7 cell line, J. Organomet. Chem 833 (2017) 80–87. doi:10.1016/j.jorganchem.2017.01.020.

[24]. İnan A, Sünbül AB, İkiz M, Tayhan SE, Bilgin S, Elmastaş M, Sayın K, Ceyhan G, Köse M, İspir E, Half-sandwich Ruthenium(II) arene complexes bearing the azo-azomethine ligands: Electrochemical, computational, antiproliferative and antioxidant properties, J. Organomet. Chem 870 (2018) 76–89. doi:10.1016/j.jorganchem.2018.06.014.

[25]. Biancalana L, Zacchini S, Ferri N, Lupo MG, Pampaloni G, Marchetti F, Tuning the cytotoxicity of ruthenium(ii) para-cymene complexes by monosubstitution at a triphenylphosphine/phenoxydiphenylphosphine ligand, Dalt. Trans 46 (2017) 16589–16604. doi:10.1039/c7dt03385k.

[26]. Tadić A, Poljarević J, Krstić M, Kajzerberger M, Aranelović S, Radulović S, Kakoulidou C, Papadopoulos AN, Psomas G, Grgurić-Šipka S, Rutheniumarene complexes with NSAIDs: Synthesis, characterization and bioactivity, New J. Chem 42 (2018) 3001–3019. doi:10.1039/c7nj04416j.

[27]. Mohan N, Mohamed Subarkhan MK, Ramesh R, Synthesis, antiproliferative activity and apoptosis-promoting effects of arene ruthenium(II) complexes with N, O chelating ligands, J. Organomet. Chem 859 (2018) 124–131. doi:10.1016/j.jorganchem.2018.01.022.

[28]. Romero-Canelón I, Pizarro AM, Habtemariam A, Sadler PJ, Contrasting cellular uptake pathways for chlorido and iodido iminopyridine ruthenium arene anticancer complexes, Metallomics 4 (2012) 1271–1279. doi:10.1039/c2mt20189e. [PubMed: 23138378]

[29]. Pazinato J, Cruz OM, Naidek KP, Pires ARA, Westphal E, Gallardo H, Baubichon-Cortay H, Rocha MEM, Martinez GR, Winnischofer SMB, Di Pietro A, Winnischofer H, Cytotoxicity of η6-areneruthenium-based molecules to glioblastoma cells and their recognition by multidrug ABC transporters, Eur. J. Med. Chem 148 (2018) 165–177. doi:10.1016/j.ejmech.2018.02.026. [PubMed: 29459276]

[30]. Sheldrick GM, SHELXL-97: An Integrated System for Solving and Refining Crystal Structures from Diffraction Data (Revision 5.1), Univ. Göttingen, Ger. (1997).

[31]. Arnaud O, Koubeissi A, Ettouati L, Terreux R, Alamé G, Grenot C, Dumontet C, Di Pietro A, Paris J, Falson P, Potent and fully noncompetitive peptidomimetic inhibitor of multidrug resistance P-glycoprotein, J. Med. Chem 53 (2010) 6720–6729. doi:10.1021/jm100839w. [PubMed: 20731360]

[32]. Gilson P, Josa-Prado F, Beauvineau C, Naud-Martin D, Vanwonterghem L, Mahuteau-Betzer F, Moreno A, Falson P, Lafanechère L, Frachet V, Coll JL, Fernando Díaz J, Hurbin A, Busser B, Identification of pyrrolopyrimidine derivative PP-13 as a novel microtubule-destabilizing agent with promising anticancer properties, Sci. Rep 7 (2017) 1–14. doi:10.1038/s41598-017-09491-9. [PubMed: 28127051]

[33]. Baiceanu E, Nguyen KA, Gonzalez-Lobato L, Nasr R, Baubichon-Cortay H, Loghin F, Le Borgne M, Chow L, Boumendjel A, Peuchmaur M, Falson P, 2-Indolylmethylenebenzofuranones as first effective inhibitors of ABCC2, Eur. J. Med. Chem 122 (2016) 408–418. doi:10.1016/j.ejmech.2016.06.039. [PubMed: 27393949]

[34]. Szewczyk P, Tao H, McGrath AP, Villaluz M, Rees SD, Lee SC, Doshi R, Urbatsch IL, Zhang Q, Chang G, Snapshots of ligand entry, malleable binding and induced helical movement in P-glycoprotein, Acta Crystallogr. Sect. D Biol. Crystallogr 71 (2015) 732–741. doi:10.1107/S1399004715000978. [PubMed: 25760620]

[35]. Stamm M, Staritzbichler R, Khafizov K, Forrest LR, AlignMe--a membrane protein sequence alignment web server, Nucleic Acids Res 42 (2014) W246–W251. doi:10.1093/nar/gku291. [PubMed: 24753425]

[36]. Šali A, Blundell TL, Comparative protein modelling by satisfaction of spatial restraints, J. Mol. Biol 234 (1993) 779–815. doi:10.1006/jmbi.1993.1626. [PubMed: 8254673]

[37]. Morris G, Huey R, AutoDock4 and AutoDockTools4: Automated docking with selective receptor flexibility, J. Comput. Chem 30 (2009) 2785–2791. doi:10.1002/jcc.21256.AutoDock4. [PubMed: 19399780]

[38]. Sanner MF, Python: A Programming Language For Software Integration And Development, J. Mol. Graph. Model 17 (1999) 55–84. doi:10.1016/S10933263(99)99999-0. [PubMed: 10660910]

[39]. Brooks BR, III CLB, Mackerell JAD, Nilsson L, Petrella RJ, Roux B, Won Y, Archontis G, Bartels C, Boresch S, Caflisch A, Caves L, Cui Q, Dinner AR, Feig M, Fischer S, Gao J, Hodoscek MWI, Karplus M, CHARMM: The Biomolecular Simulation Program B., J. Comput. Chem 30 (2009) 1545– 1614. doi:10.1002/jcc. [PubMed: 19444816]

[40]. Walker MB, Kimmel CB, A two-color acid-free cartilage and bone stain for zebrafish larvae, Biotech. Histochem 82 (2007) 23–28. doi:10.1080/10520290701333558. [PubMed: 17510811]

[41]. L. Karas B; Buckley B; Cooper KR; White, Novel High Throughput Screening of Transition Metal Based Anticancer Compounds Using Zebrafish Embryos and ICP-MS Analysis, in: Jt. Grad. Progr. Toxicol. Piscataway, NJ. Soc. Toxicol. 57th Natl. Annu. Meet, 2018.

- $[Ru(\eta^5\text{-}Cp)(PPh_3)(2,2'\text{-bipy-}4,4'\text{-dibiotin ester})]^+$ (**Ru2**) is more cytotoxic for MCF7 and MDA-MB-231 cell lines than cisplatin
- **Ru2** has exceptional selectivity as P-gp inhibitor
- LC_{50} of **Ru2** in zebrafish is 5.73 mg/L at 5 days post fertilization.

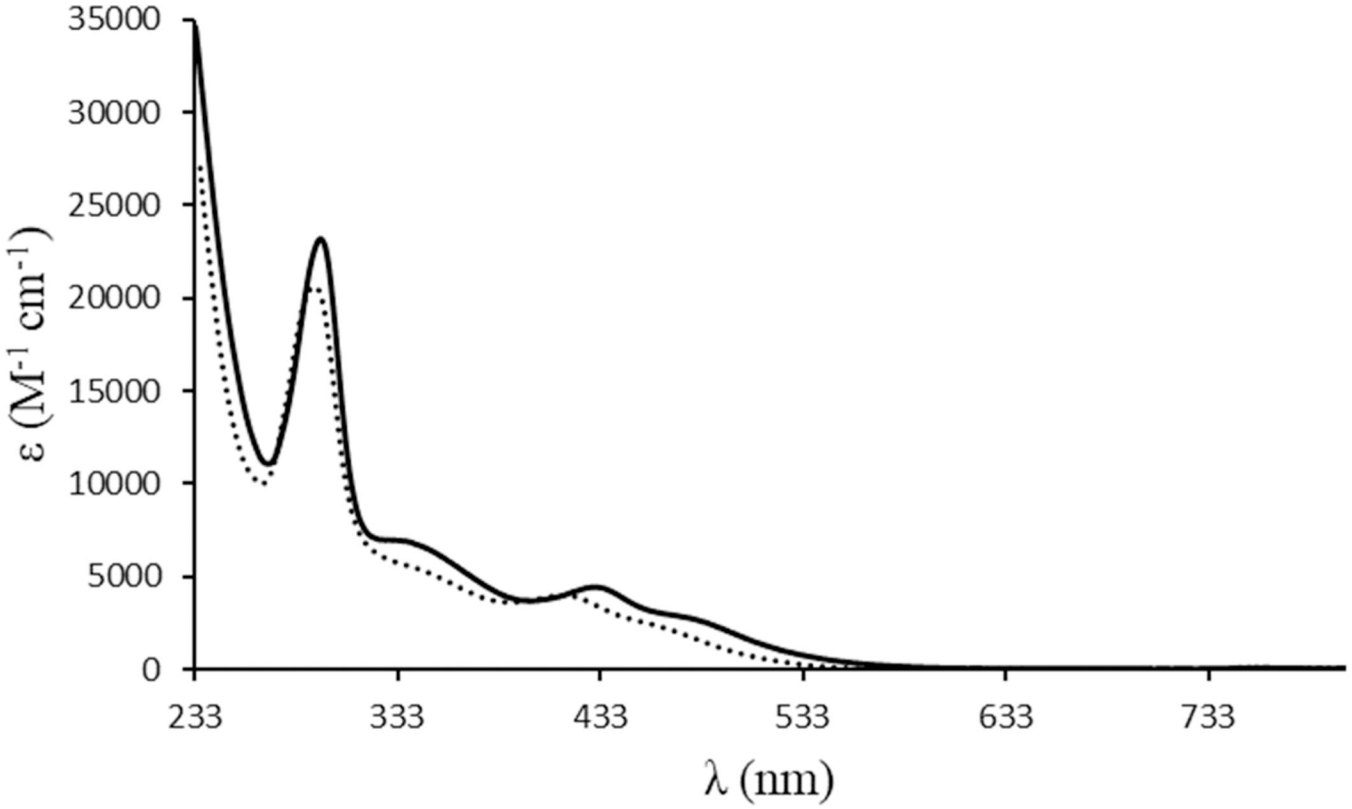

Figure 1.
Electronic spectra of complexes **Ru1** (dashed line) and **Ru2** (solid line) in dichloromethane.

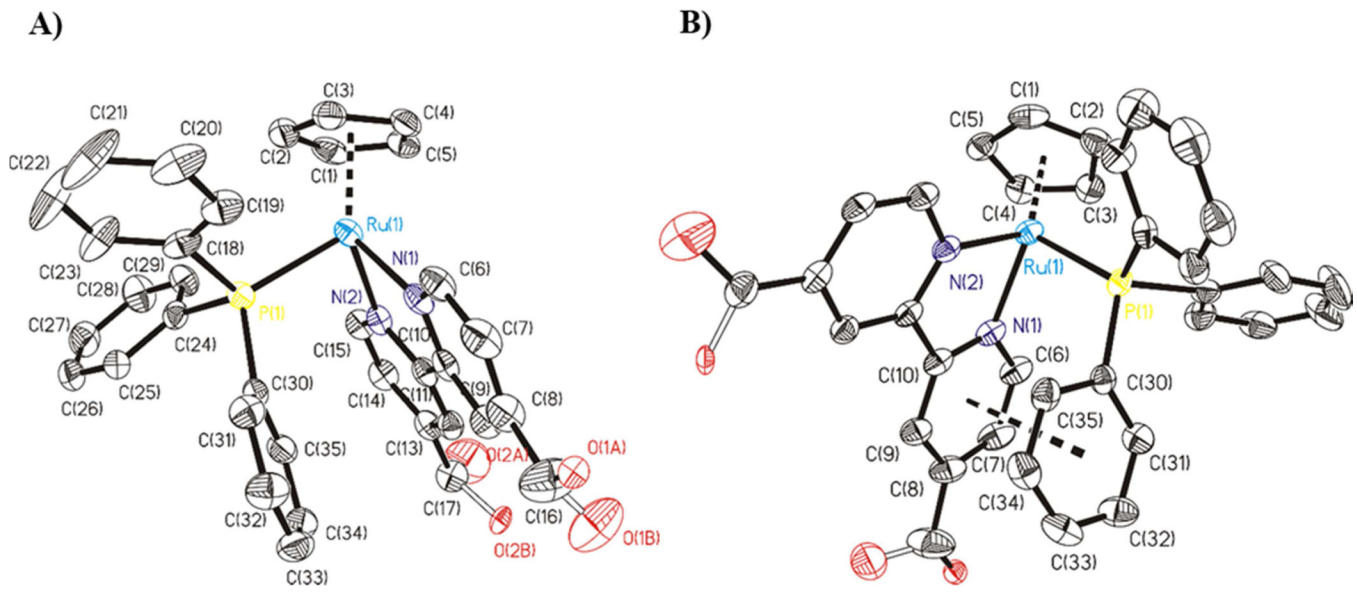

Figure 2.

A) ORTEP for the cation complex [Ru(η^5-C_5H_5)(PPh_3)(4,4'-diyldimethanol2,2'-bipyridine)]$^+$ of **Ru1**. All the non-hydrogen atoms are presented by their 50% probability ellipsoids. Hydrogen atoms are omitted for clarity; **B)** ORTEP for the cation complex [Ru(η^5-C_5H_5)(PPh_3)(4,4'-diyldimethanol-2,2'-bipyridine)]$^+$ of **Ru1** where we can see **π-π** stacking interaction between the bipyridine ring and phenyl ring of phosphane. All the non-hygrogen atoms are presented by their 50% probability ellipsoids. Hydrogen atoms are omitted for clarity.

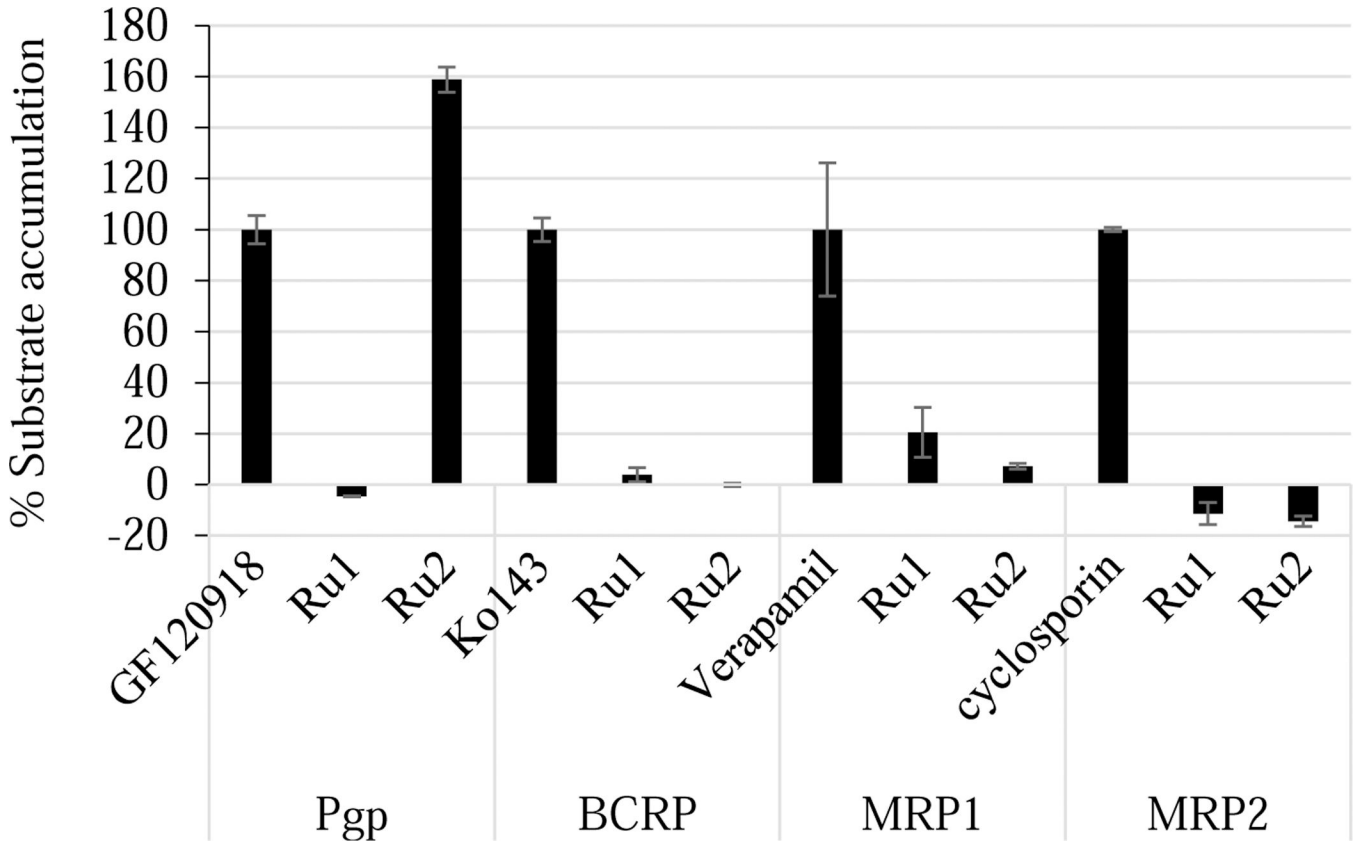

Figure 3.

Inhibition by **Ru1** and **Ru2** of MDR pumps substrate efflux. ABCG2, MRP1 and MRP2, NIH 3T3 WT and overexpressing P-gp MDR pumps are expressed as detailed in Table 4. The concentrations used for the reference substrates were: 5 μM of mitoxantrone for ABCG2, 0.5 μM of rhodamine 123 for P-gp, 0.2 μM of calcein AM for MRP1 and MRP2. **Ru1** and **Ru2** were used at 20 μM. The reference inhibitors, Ko143, GF120918, verapamil and cyclosporine A, were used at 1, 5, 325 and 325 μM, respectively.

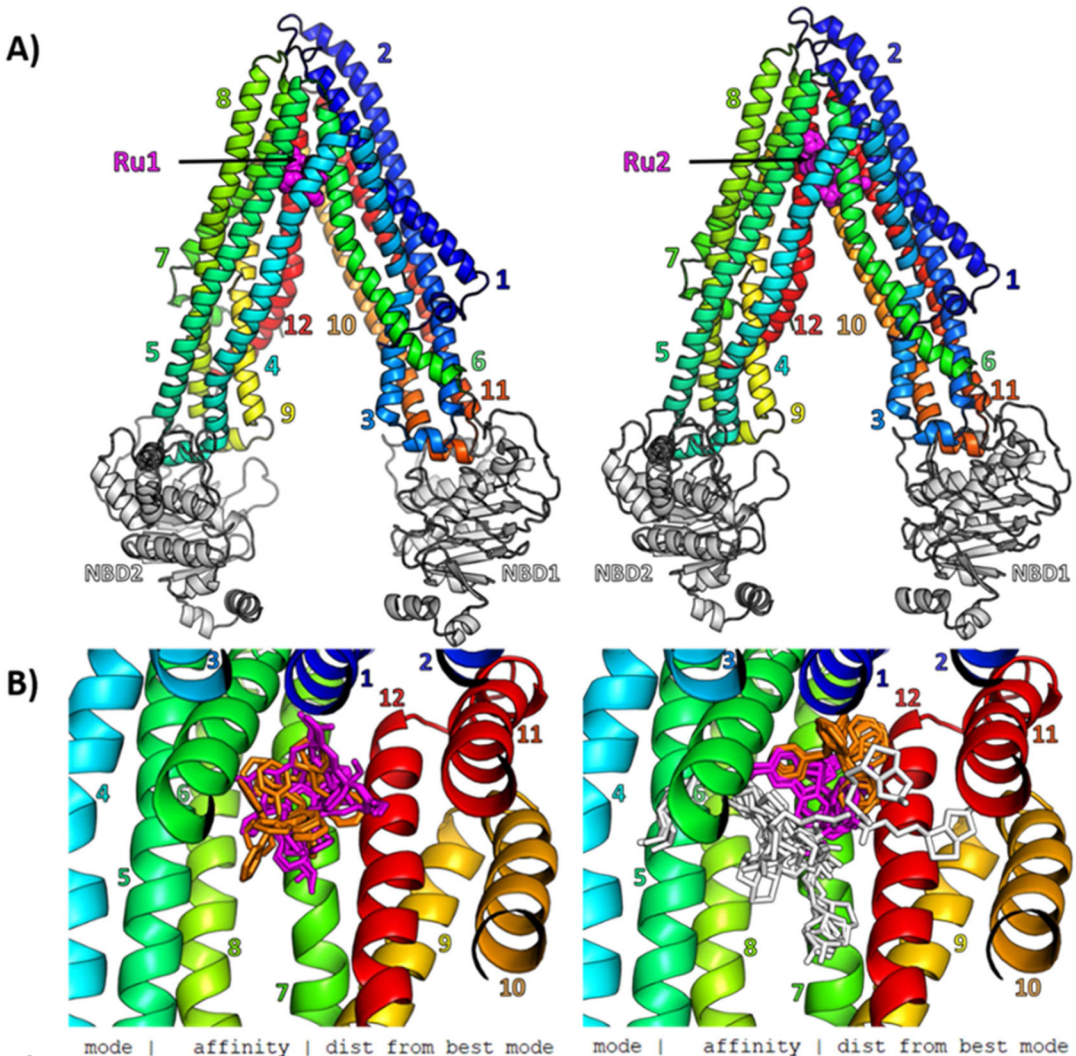

mode	affinity (kcal/mol)	dist from best mode rmsd l.b.	rmsd u.b	mode	affinity (kcal/mol)	dist from best mode rmsd l.b.	rmsd u.b.
1	-14.6	0.000	0.000	1	-18.1	0.000	0.000
2	-14.6	1.427	2.479	2	-17.9	1.431	2.589
3	-14.3	1.448	2.938	3	-17.9	1.521	2.635
4	-14.2	1.380	2.755	4	-17.8	1.585	4.817
5	-14.2	1.422	2.676	5	-17.7	1.803	4.144
6	-14.2	1.502	2.946	6	-17.7	1.416	2.295
7	-14.1	1.347	2.900	7	-17.7	1.707	4.542
8	-14.1	1.496	2.959	8	-17.6	1.839	4.478
9	-14.0	1.379	2.874	9	-17.6	1.520	2.781
10	-14.0	1.468	2.955	10	-17.6	1.640	4.640

Figure 4.

(A) Cartoon representation of human P-gp 3D model, based on the mouse Pgp crystallographic structure (PDB 4Q9H), with the best docking pose of **Ru1** and **Ru2** computed with Autodock Vina in a gridbox containing 55 flexible residues forming the drug-binding pocket. **Ru1** and **Ru2** are shown as magenta spheres, transmembrane helices are numbered and colored from blue to red, Nucleotide Binding Domains (NBD) are colored in white. **(B)** Overview of the drug-binding pocket with all 10 flexible docking poses of **Ru1** (left panel) and **Ru2**(right panel) shown as sticks with common core colored in magenta,

common PPh_3 in orange, and **Ru2** additional R-group in white. **(C)** Docking affinities and RMSD are given for all 10 flexible docking poses (or “modes”) of **Ru1** (left panel) and **Ru2** (right panel).

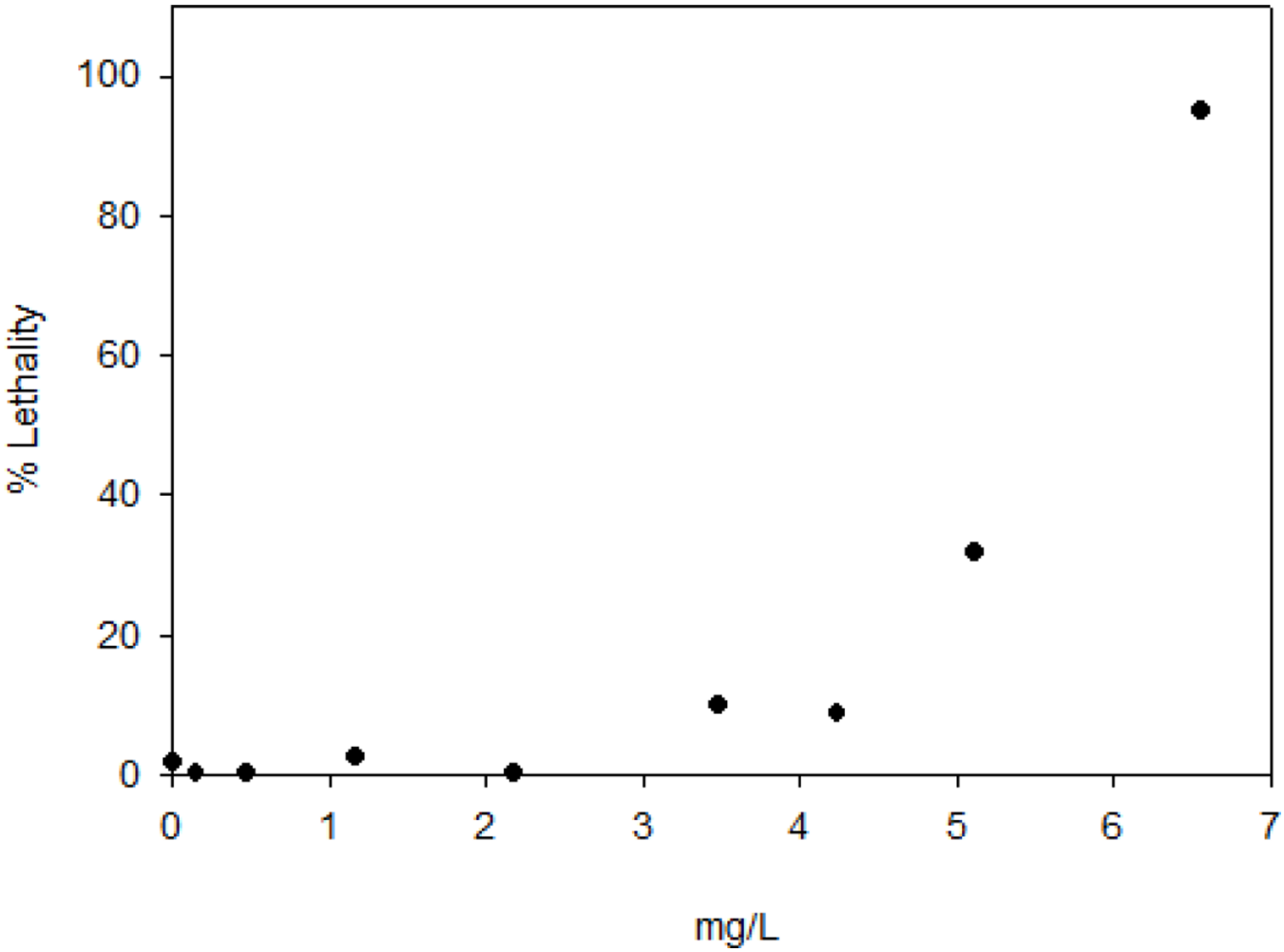

Figure 5.

Lethality-response curve for tested **Ru2** compound solutions (ND, 0.15, 0.47, 1.17, 2.18, 3.48, 4.24, 5.12 and 6.57 mg/L). ND: non-detected.

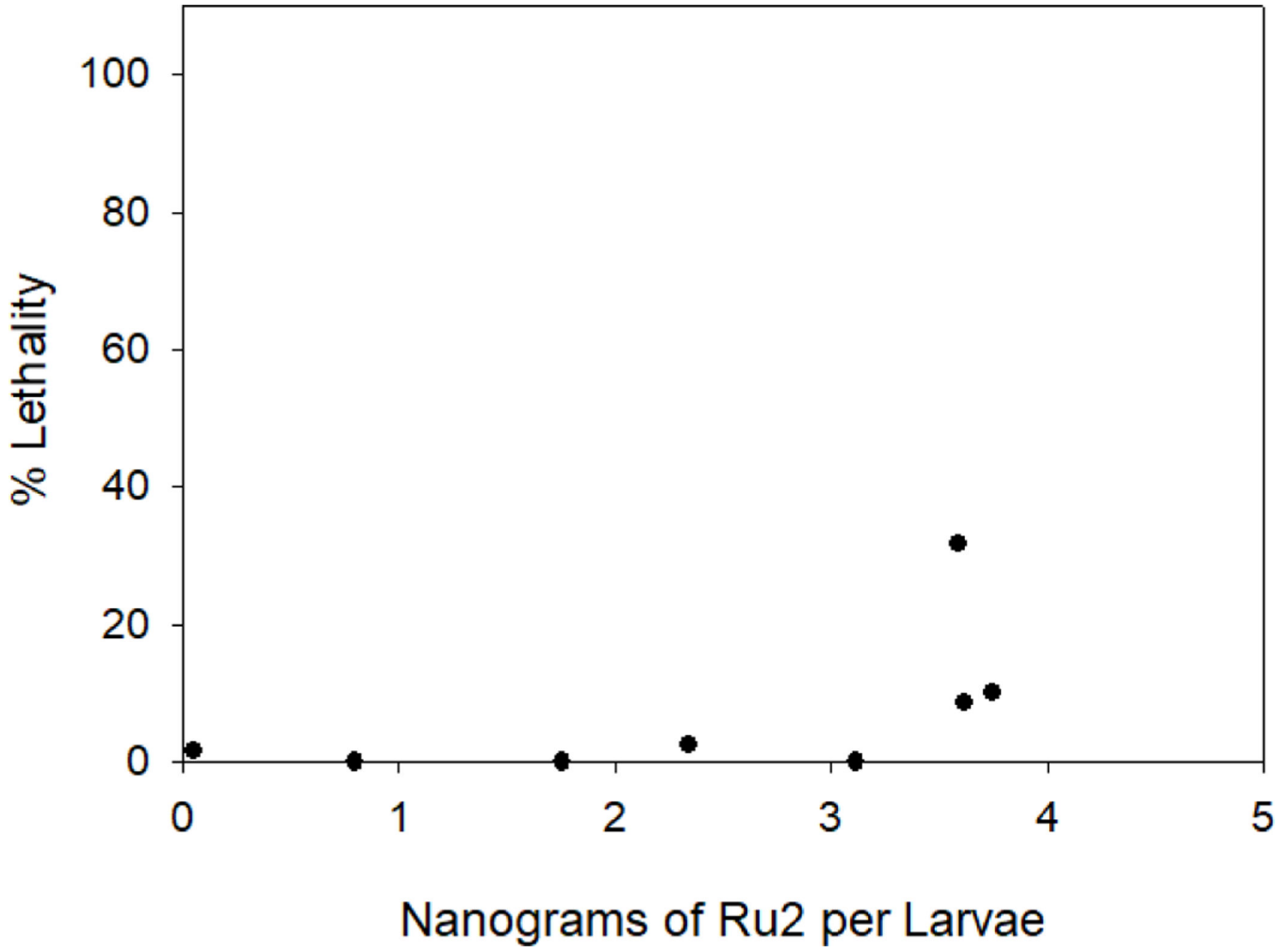

Figure 6.

Lethality-response curve for tested **Ru2** compound inside larvae in ng of **Ru2**/larvae (ND, 0.80, 1.76, 2.34, 3.11, 3.74, 3.61 and 3.59). ND: non-detected.

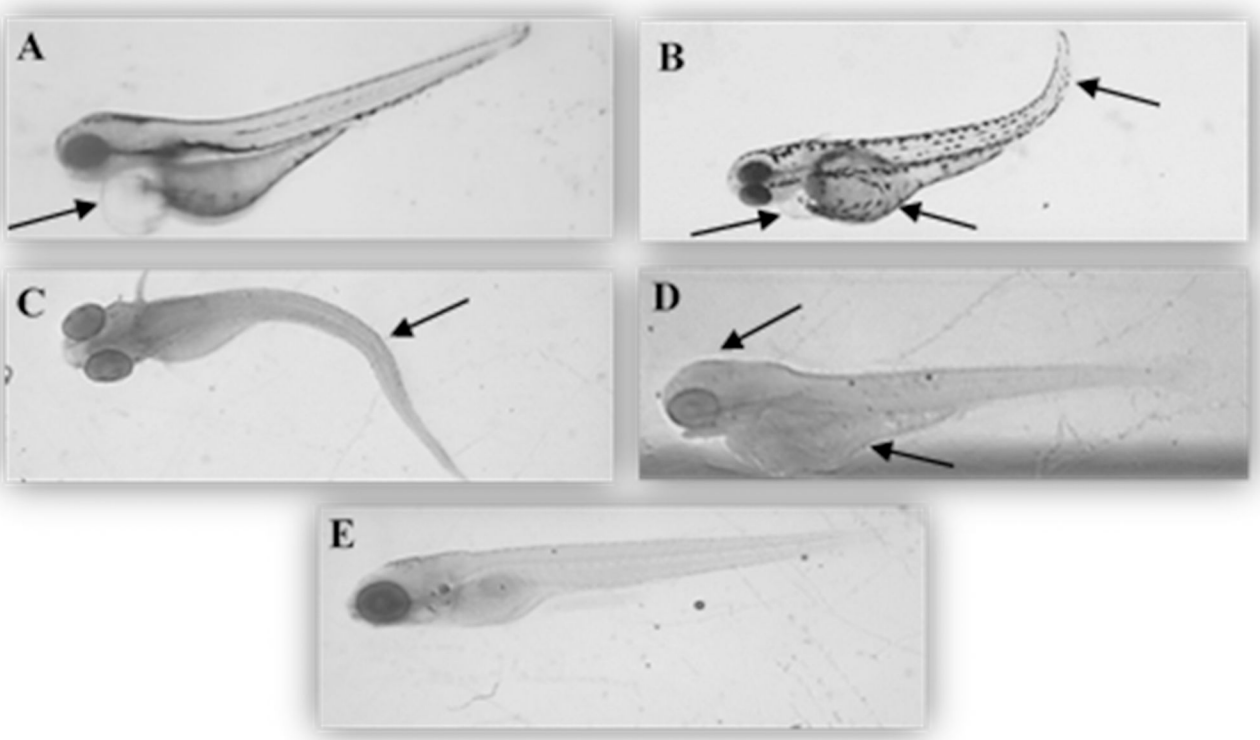

Figure 7.

Representative pictures of zebrafish lesions found at 72–120 hpf after treatment with **Ru2** complex at different concentrations (A – 2.18 mg/L and B to D – 5.12) **A:** pericardial edema; **B:** yolk sac edema, pericardial edema and curved tail; **C:** curved spine; **D:** head malformation and yolk sac edema; **E:** control. The zebrafish embryos representative pictures were obtained with Olympus SZ-PT dissecting microscope equipped with Scion digital camera model CFW-1310C and analyzed with Photoshop software. Magnification 4X.

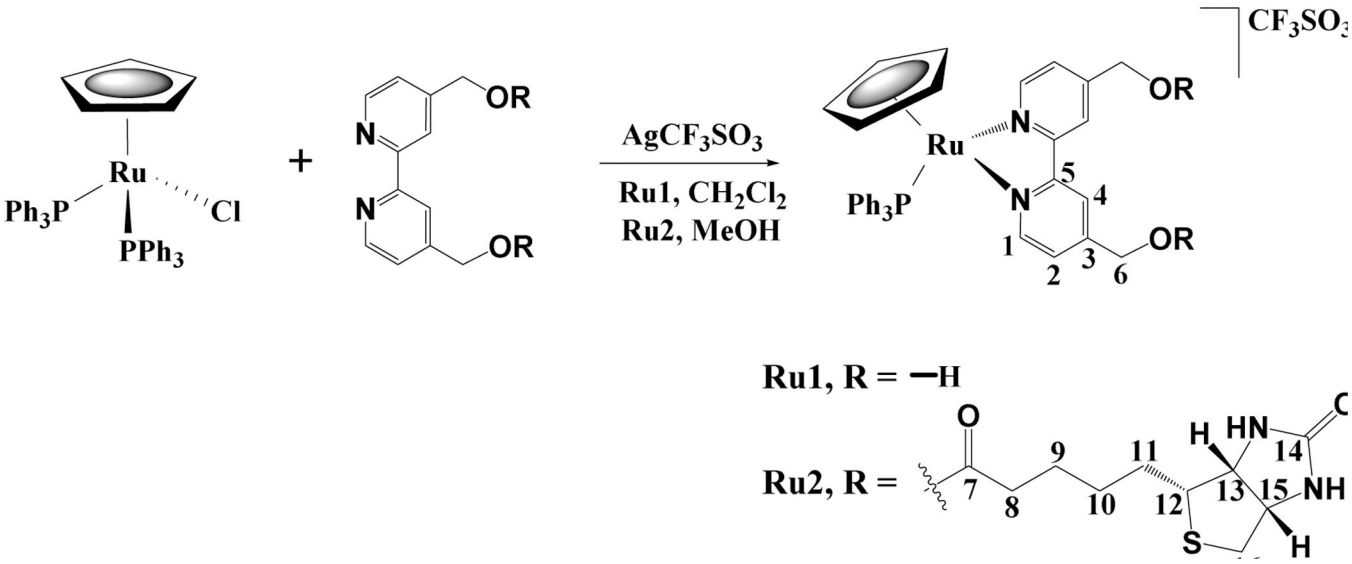

Scheme 1.

Synthetic route of the new Ru(II) complexes; all compounds are numbered for NMR assignments **Ru1**, **Ru2**.

Table 1.

Bond lengths [Å] and angles [°] for [Ru(η^5-C_5H_5)(PPh_3)(4,4'-diyldimethanol2,2'-bipyridine)][CF_3SO_3] **Ru1**.

Bond lengths	**Ru1**
Ru(1)-N(1)	2.087(3)
Ru(1)-N(2)	2.080(3)
Ru(1)-C(1)	2.175(3)
Ru(1)-C(2)	2.176(3)
Ru(1)-C(3)	2.192(3)
Ru(1)-C(4)	2.202(3)
Ru(1)-C(5)	2.208(3)
Ru(1)-P(1)	2.3098(8)
Bond angles	**Ru1**
N(2)-Ru(1)-N(1)	76.16(9)
N(2)-Ru(1)-C(1)	101.18(12)
N(1)-Ru(1)-C(1)	153.35(12)
N(2)-Ru(1)-C(5)	99.61(11)
N(1)-Ru(1)-C(5)	115.59(11)
C(1)-Ru(1)-C(5)	38.03(12)
N(2)-Ru(1)-C(2)	133.09(12)
N(1)-Ru(1)-C(2)	150.55(12)
C(1)-Ru(1)-C(2)	37.75(14)
C(5)-Ru(1)-C(2)	63.05(13)
N(2)-Ru(1)-C(4)	129.04(11)
N(1)-Ru(1)-C(4)	97.69(11)
C(1)-Ru(1)-C(4)	62.94(12)
C(5)-Ru(1)-C(4)	37.19(12)
C(2)-Ru(1)-C(4)	62.83(12)
N(2)-Ru(1)-C(3)	162.27(11)
N(1)-Ru(1)-C(3)	113.23(11)
C(1)-Ru(1)-C(3)	63.44(13)
C(5)-Ru(1)-C(3)	62.97(12)
C(2)-Ru(1)-C(3)	37.97(13)
C(4)-Ru(1)-C(3)	37.60(12)
N(2)-Ru(1)-P(1)	92.85(7)
N(1)-Ru(1)-P(1)	90.68(7)
C(1)-Ru(1)-P(1)	115.97(10)
C(5)-Ru(1)-P(1)	152.89(9)
C(2)-Ru(1)-P(1)	90.92(9)
C(4)-Ru(1)-P(1)	138.09(9)
C(3)-Ru(1)-P(1)	101.76(9)

Table 2.

Hydrogen bonds in the compound [Ru(η^5-C_5H_5)(PPh_3)(4,4'-diyldimethanol2,2'-bipyridine)][CF_3SO_3] **Ru1**.

D-H...A	d(D-H)	d(H...A)	d(D...A)	<(DHA)
O(1A)-H(1A)...O(3A)#1	0.82 Á	1.80 Á	2.350(10) Á	123.1 º
O(1A)-H(1A)...O(2A)#2	0.82 Á	2.30 Á	2.852(18) Á	125.3 º
O(2A)-H(2A)...O(2A)#3	0.82 Á	1.92 Á	2.52(2) Á	128.3 º
O(2B)-H(2B)...O(3B)#4	0.82 Á	1.84 Á	2.725(6) Á	159.3 º

Symmetry transformations used to generate equivalent atoms:

#1 -x,-y,-z+1 #2 x,y-1,z #3 -x,-y+2,-z+1 #4 -x,-y+1,-z+1

Table 3.

IC_{50} (μM) for both ruthenium complexes with a range between 0.1–100 μM, at 24 h incubation, in MCF7 and MDA-MB-231 cancer cells.

	MCF7 (μM)	MDA-MB-231 (μM)
Ru1	4.61 ± 0.96	13.9 ± 2.8
Ru2	31.5 ± 4.7	11.6 ± 1.5
Cisplatin	38 ± 1.41	122 ± 25

Table 4.

In vitro cytotoxic activity of ruthenium complexes in cell lines transfected with an empty plasmid (HEK293, NIH3T3) or overexpressing ABC transporters (P-gp, MRP1, MRP2, BCRP) after 48 h incubation at 37 °C. Compounds concentration required to inhibit 50% of the cell's growth (half maximal inhibitory growth concentration or IG_{50}) was measured by MTT assay.

	Half inhibitory growth concentration, IG_{50} (μM)			
	NIH3T3 / P-gP	**HEK293 / MP1**	**HEK293 / MRP2**	**HEK293 / BCRP**
Rul	28.1±1.2 / 67.8±3.5	4.8±0.1 / 10±0.4	4.5±1.0 / 4.9±0.9	6.7±0.2 / 19.1±0.6
Ru2	7.3±0.2 / 7.3±0.3	1.6±0.9 / 1.7±1.2	5.7±2.3 / 3.0±l.2	5.6±2.9 / l.l±0.4

Table 5.

Estimates obtained from *in vivo* toxicity analyses at the end of the 120 hpf experiment.

	LC_{50} (95% CL[a]) (mg/L)	NOEC (mg/L)	LOEC (mg/L)	NOAEL (mg/L)	NOAEL (ng/larvae)	NOEL (mg/L)	NOEL (ng/larvae)
Ru2	5.73 (4.74–6.26)	2.18	3.48	2.18	3.11	1.17	2.34

[a]CL = confidence limits; NOEC - no observed effect concentration; LOEC - lowest observed effect concentration; NOEL – no observed effect level; NOAEL – No observed adverse effect level.

Table 6.

Crystal data and structure refinement for [Ru(η^5-C_5H_5)(PPh_3)(4,4'diyldimethanol-2,2'-bipyridine)][CF_3SO_3] **Ru1**.

	Ru1
Formula	C_{36} H_{32} F_3 N_2 O_5 P Ru S
Formula weight	793.74
T, *K*	100(2)
Wavelength, Å	0.71073
Crystal system	Triclinic
Space group	P 1
a/Å	11.4703(6)
b/Å	11.6069(6)
c/Å	13.4443(7)
α/°	75.737(3)
β/°	81.039(3)
γ/°	69.653(3)
V/Å^3	1621.64(15)
Z	2
F000	808
D_{calc}/g cm^{-3}	1.626
μ/mm^{-1}	0.663
θ/(°)	1.57 to 25.19
R_{int}	0.0431
Crystal size/ mm^3	0.37 × 0.25 × 0.10
Goodness-of-fit on F^2	1.132
R_1 [a]	0.0315
wR_2 (all data) [b]	0.0973
Largest differences peak and hole (eÅ^{-3})	0.854 and −0.748

[a] $R1 = \Sigma||F_O| - |F_C||/\Sigma|F_O|$.

[b] $wR2 = \{\Sigma[w(|F_O|^2 - |F_C|^2|)^2]/\Sigma[w(F_O^2)^2]\}^{1/2}$

Table 7.

ICP-MS Method

Method Settings	***Parameter***
Analysis Mode	Deflector Jump, single mass jump
Dwell Time Per Peak	4 ms
Switch Delay Per Peak (×10 us)	2
Number Sweeps	450
Number of Cycles	1
Instrument Resolutuion	300
Scan Window (%)	0
Peak Center Mass	None
Detection Mode	Attenuated
Park Mass	98.90594